

# UC Davis

## UC Davis Previously Published Works

### Title

Deep Structural Analysis and Quantitation of O-Linked Glycans on Cell Membrane Reveal High Abundances and Distinct Glycomic Profiles Associated with Cell Type and Stages of Differentiation.

### Permalink

<https://escholarship.org/uc/item/8k24w22m>

### Journal

Analytical Chemistry, 92(5)

### Authors

Xu, Gege

Goonatilleke, Elisha

Wongkham, Sopit

et al.

### Publication Date

2020-03-03

### DOI

10.1021/acs.analchem.9b05103

Peer reviewed



Published in final edited form as:

*Anal Chem.* 2020 March 03; 92(5): 3758–3768. doi:10.1021/acs.analchem.9b05103.

## Deep structural analysis and quantitation of O-linked glycans on cell membrane reveal high abundances and distinct glycomic profiles associated with cell type and stages of differentiation

Gege Xu<sup>1,5</sup>, Elisha Goonatileke<sup>1,5</sup>, Sopit Wongkham<sup>4</sup>, Carlito B. Lebrilla<sup>\*,1,2,3</sup>

<sup>1</sup>Department of Chemistry, University of California, Davis, CA 95616, USA

<sup>2</sup>Department of Biochemistry and Molecular Medicine, University of California, Davis, CA 95616, USA

<sup>3</sup>Foods for Health Institute, University of California, Davis, CA 95616, USA

<sup>4</sup>Department of Biochemistry, Faculty of Medicine, Khon Kaen University, Khon Kaen 40002, Thailand

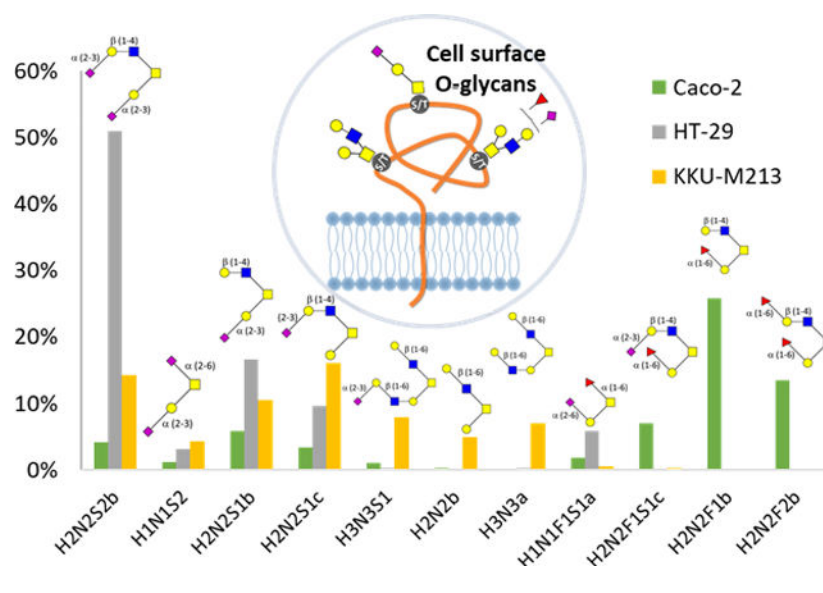
### Abstract

Proteins on cell membrane are modified by N- and O-glycans. N-Glycans have been extensively characterized using advanced separation and mass spectrometry techniques. However, O-glycans remain a challenge due to the lack of universal enzyme to release them and the large background abundances of N-glycans. Here, we report a method for in-depth structural analysis and quantitation of O-glycans derived from human cell membrane. O-Glycans were chemically released from isolated cell membrane glycoproteins following N-glycan and lipid/glycolipid removal by PNGase F digestion and Folch extraction, respectively. Released O-glycans were purified by an optimized protocol to eliminate interference from small molecules and degraded proteins. Cell surface O-glycans were then analyzed using a nanoLC-chip-QTOF mass spectrometer with a porous graphitized carbon (PGC) column while the N-glycans and glycolipids isolated from the same cell membrane fractions were analyzed in parallel using previously reported methods. The monosaccharide compositions and linkages of the detected O-glycans were identified by exoglycosidase digestion facilitated with tandem MS. Using this method, we identified 44 cell membrane O-glycan isomers with tandem MS, and among them we unambiguously characterized 25 O-glycan structures with exoglycosidase digestion to create a library with their complete structures, accurate masses and retention times. In this process, we identified and characterized unexpected mannose oligomers that are  $\alpha(1-2/3)$  linked. This library enabled the identification and quantification of unique cell surface O-glycans from different cell lines and the study of specific O-glycan changes during cell differentiation.

### Graphical Abstract

\*To whom correspondence should be addressed. Carlito B. Lebrilla, University of California, Davis, Department of Chemistry, One Shields Avenue, Davis, CA, 95616, USA. cblebrilla@ucdavis.edu.

<sup>5</sup>These authors contributed equally to this work



## Introduction

Glycosylation is one of the most structurally complicated but common post-translational modifications (PTMs) on proteins, and it involves the covalent attachment of glycans to specific amino acids.<sup>1</sup> The majority of human proteins are modified with the two common types of glycosylation, N- and O-glycosylation. With N-glycosylation, glycans are attached to the asparagine residues while in O-glycosylation, glycans are attached to either serine, threonine, or tyrosine residues.<sup>2</sup> O-Glycans are categorized into two groups, mucin and non-mucin, depending on the monosaccharide residue attached to the amino acid. In mucin-type O-glycans, N-acetylgalactosamine (GalNAc) attaches to the amino acid residue whereas non-mucin type O-glycosylation is initiated by attaching N-acetylglucosamine (GlcNAc), mannose, fucose, glucose, galactose, or xylose onto the amino acid.<sup>3</sup> Among these glycan types, O-GalNAc and O-GlcNAc have gained much attention due to their biological importance.<sup>4</sup> Further sequential additions particularly to O-GalNAc of monosaccharides such as GlcNAc, galactose, sialic acid and fucose by a variety of glycosyltransferases further elongate the O-glycan structures and make them more heterogeneous.

Mucin-type O-glycans can be categorized into eight groups based on their core structures, and Core 1 and Core 2 are the two most common types observed in humans.<sup>2, 5</sup> Changes in cell surface glycans are found to be associated with the pathological state making them targets for disease biomarker discovery.<sup>6-9</sup> Mucin-type O-glycans on cell membrane are known to play an important role in cell signaling, cell adhesion, conformation, stability, solubility, and tumorigenesis.<sup>5, 10-13</sup> In gastric cancer patients for example, an elevated level of serum O-glycans was observed.<sup>14</sup> O-glycans were also reported to play two opposing roles in tumor metastasis depending on their structures: Core 2 O-glycans allow tumor survive longer in the circulatory system while Core 3 O-glycans suppress tumor formation and metastasis.<sup>15</sup> Overexpression of ST3GalII leading to the increased expression of sialylated Core 1 O-glycans on tumor cell membrane led to increased tumor growth in breast cancer.<sup>16-17</sup> However, these studies are commonly conducted using lectins, lacking

information on the functions of specific O-glycan structures. Therefore, deep knowledge of the mucin-type O-glycan structures including the linkage of each monosaccharide residue is essential.

Despite the importance of cell surface O-glycans, there is only limited knowledge of their structures and abundances, particularly compared to N-glycans. Characterization of cell surface glycosylation was normally performed using one of these two strategies: release and analyze only the glycans, and analyze intact glycolipids and glycopeptides.<sup>18–19</sup> Released glycans were usually separated by HPLC and detected by UV or fluorescence detectors after derivatization.<sup>20–22</sup> However, the maximum number of glycans that can be monitored using this approach was limited by the peak capacity of chromatographic methods as quantitation relied on baseline separation of all glycans. The accuracy of quantitation may also be affected by impurities in the sample matrices. Alternatively, the released glycans were analyzed using MALDI-MS or LC-ESI-MS after permethylation or derivatization of the reducing end.<sup>23–27</sup> While derivatization such as permethylation could improve the ionization efficiency, they often introduced higher variability during the sample preparation due to the additional chemical steps and incomplete reactions. In addition, the permethylated glycan products yielded poor isomeric separation.<sup>28</sup> For comprehensive mapping of glycans, highly sensitive and quantitative methods employing electrospray ionization (ESI) in conjunction with nano-LC separation with porous graphitized carbon (PGC) stationary phase and MS detection have been developed. This approach have been used extensively by our group to characterize N-glycans released from serum and cell surface glycoproteins to discover cancer biomarkers and study membrane protein functions.<sup>29–32</sup> Owing to the specific interactions of glycans with PGC, N-glycan isomers were extensively separated. The enrichment column and nanospray features of the chip platform also provided efficient removal of contaminants and high sensitivity that enabled detection of ultra-low abundance glycan isomers.

Despite the advancements in glycan analysis, characterization of O-glycans remains more challenging compared to N-glycans for several reasons. In contrast to N-glycosylation, O-linked glycoproteins do not carry a consensus amino acid sequence for the glycosylation site, which complicates the analysis of O-glycosylation sites on proteins.<sup>33</sup> The heterogeneity in glycan structures and lack of enzymes to release different types of O-glycans from glycoproteins makes the analysis even more difficult.<sup>4</sup> Nevertheless, several analytical platforms including lectin affinity chromatography, high-performance liquid chromatography and capillary electrophoresis coupled to mass spectrometry have been used in the analysis of O-glycans.<sup>34–35</sup> For example, Morelle et al studied the structures of permethylated N- and O-glycans released by PNGase F and reductive  $\beta$ -elimination.<sup>36</sup> Yang et al developed a similar approach to release the glycans after immobilizing proteins onto an aldehyde-active solid support by reductive amination.<sup>37</sup> Although solid support facilitated sample cleanup, consistent and high degree of conjugation efficiency was a prerequisite for quantitative analysis of glycans from the samples.<sup>38</sup>

In this study, we report a deep and comprehensive glycomic platform for characterizing cell surface O-glycans from a variety of cell lines including Caco-2, HT-29, and KKU-M213 cells using nanoLC-chip-QTOF-MS. O-Glycans were released using  $\beta$ -elimination and

purified using a two-step cleanup process which was optimized specifically for cell line and tissue samples. This analysis allows identification of O-glycans at an isomeric level by including linkages for sialic acids and fucose residues. Our study reports the most comprehensive and complete O-glycan structures identified thus far including twenty-five abundant structures on the cell surface. Application of this method to characterize cell surface O-glycans from multiple cell lines shows the highly specific glycosylation profiles of different cell types.

## Experimental Section

### Cell Culture

Human colorectal adenocarcinoma Caco-2 cells were obtained from American Type Culture Collection (ATCC, VA) and grown in Eagle's Minimum Essential Medium (Gibco, Thermo Fisher Scientific, MA). To study the changes of Caco-2 cell surface glycans during differentiation, the cells were harvested at different growth time points on days 5, 7, 14, 21, and 24 by scraping with four biological replicates for each time point. Human colorectal adenocarcinoma HT-29 cells were obtained from ATCC and grown in McCoy's 5A medium (Gibco, Thermo Fisher Scientific, MA). HT-29 cells were partially differentiated 4-days post-confluency and collected by scraping. Human cholangiocarcinoma KKU-M213 cells were obtained from the Japanese Collection of Research Bioresources Cell Bank (JCRB, Osaka, Japan), grown in Ham's F12 medium (Gibco, Thermo Fisher Scientific, MA), and harvested at 80–90% confluency by scraping. All the culture media were supplemented with 10% (v/v) fetal bovine serum, and 100 U/mL penicillin and streptomycin. Cells were subcultured at 80% confluency maintained at 37°C in a humidified incubator with 5% CO<sub>2</sub>.

### Cell Membrane Extraction

Extraction of the cell membrane compartment was performed as described previously with modified procedures.<sup>39–40</sup> In brief, harvested cells were resuspended in homogenization buffer containing 0.25 M sucrose, 20 mM HEPES-KOH (pH 7.4), and 1:100 protease inhibitor (EMD Millipore, CA). Cell lysis was performed on ice using a probe sonicator (Qsonica, CT) with five alternating on and off pulses in 5 and 10 s intervals, respectively. Lysates were centrifuged at 2,000 x g for 10 min to remove the nuclear fractions and cellular debris. The supernatant was collected for ultracentrifugation at 200,000 x g for 45 min at 4°C. The pellet was resuspended and repelleted by ultracentrifugation using the same conditions in 0.2 M Na<sub>2</sub>CO<sub>3</sub> followed by water to fragment the endoplasmic reticulum and remove the cytoplasmic fraction, respectively. The resulting membrane fraction was isolated and stored at –20°C until further processing.

### Enzymatic Release of N-Glycans

N-Glycan release procedure was described previously.<sup>29–30</sup> Membrane pellets were resuspended with 100 µL of 100 mM ammonium bicarbonate in 5 mM dithiothreitol and heated for 10 s in boiling water bath to denature the proteins thermally. To cleave the N-glycans from membrane proteins, 2 µL of peptide N-glycosidase F (New England Biolabs, MA) was added to the samples and incubated at 37°C in a microwave reactor (CEM Corporation, NC) for 10 min at 20 watts. After addition of 350 µL of nanopure water,

samples were ultracentrifuged at 200,000 x g for 45 min at 4°C to precipitate the membrane fractions with lipids and residual deglycosylated proteins for subsequent O-glycan and glycolipid analyses. Supernatant containing released N-glycans was desalted using porous graphitized carbon solid-phase extraction (SPE) in a 96-well plate (Glygen, MD).

### Chemical Release and Purification of O-Glycans

The membrane fraction after N-glycan release was suspended in 500 µL of Folch solvent containing water, methanol, and chloroform (v/v/v = 3/8/4) and centrifuged at 21,000 x g for 3 min to precipitate the deglycosylated proteins. The precipitated proteins were washed with 500 µL of the same Folch solvent and dried *in vacuo*. After addition of 90 µL of nanopure water, the dried protein pellet was sonicated for 20 min to resuspend the proteins. The suspended proteins were then mixed with 10 µL of 2 M NaOH and 100 µL of 2 M NaBH<sub>4</sub> and incubated at 45 °C for 18 h. The reaction was quenched by adding 10 % acetic acid on ice until the pH reached 5 to 7. After centrifugation at 21,000 x g for 20 min, the supernatant containing free O-glycans was loaded onto a PGC-SPE 96-well plate (Glygen, MD) conditioned with a solution of 80% (v/v) acetonitrile and 0.1% (v/v) trifluoroacetic acid in water and equilibrated with nanopure water. The samples were then washed with nanopure water and eluted with a solution of 40% (v/v) acetonitrile and 0.05% (v/v) trifluoroacetic acid in water. The eluted O-glycans were dried, reconstituted in 89% (v/v) acetonitrile with 1% (v/v) trifluoroacetic acid in water and further purified by iSPE-HILIC cartridges (Nest Group, MA). The cartridges were conditioned with acetonitrile, 0.1% (v/v) trifluoroacetic acid in water, and 89% (v/v) acetonitrile with 1% (v/v) trifluoroacetic acid in water. Sample was loaded onto the column, and the flow-through was collected and reloaded two times. The column was then washed with 89% (v/v) acetonitrile with 1% (v/v) trifluoroacetic acid in water. The purified O-glycans were eluted with a solution of 0.1% (v/v) trifluoroacetic acid in water and dried *in vacuo* before they were reconstituted in 90 µL of nanopure water and analyzed by LC-MS/MS.

### Glycomic Analysis by LC-MS/MS

For both N-glycan and O-glycan analysis, 5 µL of reconstituted sample from each cell line or pooled sample from all cell lines was injected to an Agilent nanoLC-chip-QTOF-MS system (Agilent Technologies, CA). Samples were introduced into the MS with a microfluidic chip, which consisted of an enrichment column and an analytical column (43 × 0.075 mm i.d.) packed with porous graphitized carbon with a 5 µm pore size, and a nano-electrospray tip. The aqueous mobile phase A was 3% (v/v) acetonitrile and 0.1% (v/v) formic acid in water, and the organic mobile phase B was 90% (v/v) acetonitrile in 1% (v/v) formic acid in water. Samples were loaded onto the enrichment column with a loading pump using 1% B at 3 µL/min for three minutes before switching to the analytical column. The glycans were then separated and eluted at a flow rate of 0.3 µL/min with a binary gradient of 0.0–2.5 min, 1% B; 2.5–20.0 min, 1–16% B; 20.0–30.0 min, 16–44% B; 30.0–35.0 min, 44–100% B. The columns were then washed with 100% B for 10 minutes and equilibrated with 1% B for 15 minutes. The MS parameters included a drying gas temperature and flow rate set at 325 °C and 5 L/min, respectively. The fragmentor voltage was set at 175 V. The capillary voltage was adjusted between 1800 V and 2000 V to maintain stable electrospray. MS spectra were acquired over a mass range of *m/z* 600–2000 for N-glycans and *m/z* 300–

2000 for O-glycans in positive ionization mode. MS/MS spectra were acquired over a mass range of  $m/z$  100–2000. Both MS and MS/MS were set at 1.5 s per spectrum with mass resolution of 14000. The isolation window of quadrupole was 1.3 Da. Mass inaccuracies were corrected with reference mass  $m/z$  1221.991. Collision-induced dissociation (CID) was performed with nitrogen gas using a series of collision energies ( $V_{\text{collision}}$ ) dependent on the  $m/z$  values of the glycans, based on the equation:  $V_{\text{collision}} = m/z (1.8/100 \text{ Da}) V - 2.4 \text{ V}$ , where the slope and intercept were optimized to obtain maximum glycan structural information from MS/MS data.<sup>41</sup>

### Fractionation of O-Glycans using HPLC

Pooled O-glycans from all cell lines were fractionated off-line using an Agilent Hewlett-Packard Series 1100 HPLC system as previously reported.<sup>42</sup> Glycans were separated using a Hypercarb PGC column (Thermo Scientific) (100 mm X 0.5 mm inner diameter, 5  $\mu\text{m}$  particle size) with a 80-min binary gradient consisting of solvent A of 3% ACN, 0.1% FA and solvent B of 90% ACN, 0.1% FA in pure water (v/v) at a flow rate of 0.3 mL/min. A total of 120 fractions were collected (one fraction every 0.5 min from 0 min to 60 min). Fractions were dried *in vacuo* and reconstituted in 20  $\mu\text{l}$  of nanopure water before analyzing with nanoLC-chip-QTOF-MS.

### Exoglycosidase Digestion of O-Glycans

A variety of exoglycosidases have been used to elucidate the structures of O-glycans as previously reported.<sup>43</sup> In brief, 0.1 M ammonium acetate reaction buffer was prepared and the pH was adjusted for different enzymes by adding glacial acetic acid. In exoglycosidase digestion, 6  $\mu\text{l}$  of buffer, 2  $\mu\text{l}$  of an O-glycan fraction, and 1  $\mu\text{l}$  of exoglycosidase were mixed and incubated at 37  $^{\circ}\text{C}$ . (Supplemental Table 1). The reaction times were optimized by monitoring the completion of reaction at different time points. The reaction times used in this study for various exoglycosidase digestion were similar to previously reported studies.<sup>42–43</sup> O-Glycans in each reaction was monitored before and after digestion using LC-MS with the same separation gradient as described above.

## RESULTS AND DISCUSSION

### Workflow for O-glycan Analysis

A workflow for comprehensive characterization of the cell glycocalyx is shown in Supplemental Figure 1. For each cell sample, plasma membrane fraction was extracted using an optimized protocol<sup>44</sup> and separated to two portions for glycomic, and proteomic and glycoproteomic analyses, respectively. Because PNGase F is highly specific for N-glycans, O-glycans are still attached to the proteins after N-glycan release. Therefore, after PNGase F digestion, the remaining membrane fraction from the same sample could be pelleted via ultracentrifugation and subjected to a modified Folch extraction procedure for parallel glycolipid<sup>45</sup> and O-glycan analyses. The other portion of the same sample was stored for proteomic or glycoproteomic analysis, as reported.<sup>35</sup> To achieve reproducible and comprehensive glycomic profiles of plasma membrane proteins, the sample preparation procedures for the preparation and purification of O-glycans were optimized in this study.

Compared to N-glycans, the analysis of O-glycans is more challenging due to the lack of specific and universal enzymes that can release the O-glycans from glycoproteins. Other components of plasma membrane further increase the difficulty in purifying the released O-glycans. In this study, the membrane fractions were subjected to a modified Folch extraction to precipitate the de-N-glycosylated proteins. This step not only enabled the isolation of glycolipids for subsequent LC-MS/MS analysis, but also facilitated the removal of lipids, the major component of plasma membrane that may interfere with the purification of O-glycans. Cell surface O-glycans were released from the precipitated proteins by a reductive  $\beta$ -elimination reaction using sodium hydroxide and sodium borohydride. Immediate reduction after  $\beta$ -elimination stabilized the released O-glycans and reduced degradation due to peeling reactions.<sup>34</sup> However, this chemical release method would also degrade the polypeptide chain, generating a large amount of small peptides. As shown in Supplemental Figure 2a–b, when only porous graphitized carbon solid-phase extraction (PGC SPE) was used to purify the released O-glycans, the overall intensity of the total ion chromatogram reached  $10^7$  while only a few O-glycans were identified possibly due to the ion suppression caused by peptides. Although another commonly used cleanup method, HILIC SPE, was efficient in washing out the salts and small peptides, the large amount of impurities in the sample affected the effective binding of O-glycans that most of the neutral glycans were lost. (Supplemental Figure 2c–d) To avoid the ion suppression and enhance the enrichment efficiency for O-glycans, we optimized the purification approach using a two-step SPE process. PGC SPE was used first to remove the sodium salts introduced during the chemical release reaction. HILIC-SPE was then performed to remove small peptides produced during  $\beta$ -elimination. Purified O-glycans were analyzed by a chip-based Q-TOF LC-MS/MS instrument using PGC as the stationary phase and identified by spectral searching using an in-house library. With optimal solvents and washing procedure, the number of detected compounds from Caco-2 cell based on accurate mass searching was increased from seven (PGC SPE only) to over one hundred (Supplemental Figure 2e–f).

### Characterization of O-glycans by MS and MS/MS

To produce a comprehensive O-glycan library, the released O-glycans from the cell lines were pooled for further analysis. Supplemental Figure 3 shows the extracted compound chromatograms of O-glycans in the pool identified by matching their accurate masses (mass tolerance less than 10 ppm) and isotope patterns with an O-glycan compositional library using the molecular feature finding function in MassHunter Qualitative Analysis B.07 software (Agilent, CA). Over 100 glycan compositions corresponding to >200 glycan structures (isomers included) spanning over five orders of magnitude in dynamic range were detected based on MS1 matching with the compositional library. The monosaccharide compositions of the most abundant species were annotated.

Tandem MS was used as a rapid method for obtaining monosaccharide composition information and differentiating the isomers thereby adding an extra level of validation to the structural analysis.<sup>41, 46–47</sup> Tandem MS yielded fragmentation pathways that guided the partial elucidation of structures. Figure 1 shows the MS/MS spectra of two fucosylated isomers Hex<sub>2</sub>HexNAc<sub>2</sub>Fuc<sub>1</sub>NeuAc<sub>1</sub> (H2N2F1S1a and H2N2F1S1b). For both isomers, an initial loss of sialic acid was observed indicating that the sialic acid was attached to



the terminal hexose of the glycan structures. However, a fragment ion  $m/z$  of 803.56 corresponding to Hex<sub>1</sub>HexNAc<sub>1</sub>Fuc<sub>1</sub>NeuAc<sub>1</sub> with no reducing end was only detected for H2N2F1S1b (Figure 1b). This confirmed the presence of both sialic acid and the fucose in the same antenna of the glycan with the fucose attached to a HexNAc residue. Nevertheless, the exact connectivity between the monosaccharide residues for this isomer could not be confirmed by MS/MS data only. Two possible structures for H2N2F1S1b are shown in Figure 1b. The exact structures and monosaccharide linkages of this O-glycan were further elucidated by exoglycosidase digestion and shown in Table 1. In Figure 1a, however, a different fragmentation pattern for isomer H2N2F1S1a was observed. We identified fragment ions corresponding to the initial loss of sialic acid and fucose in the fragmentation pathways indicating the presence of sialic acid and fucose residues at the non-reducing terminus of the glycan structure. Additionally, the data contained fragments corresponding to Hex<sub>1</sub>HexNAc<sub>1</sub>Fuc<sub>1</sub> ( $m/z$  512.20) and Hex<sub>1</sub>HexNAc<sub>1</sub>NeuAc<sub>1</sub> with reducing end ( $m/z$  677.25), indicating the fucose residue is attached to the elongated antenna of Core 2 structure, and the sialic acid is attached to the other antenna of the glycan.

Instead of manually interpreting the monosaccharide compositions of the cell surface O-glycans, we utilized an in-house software to annotate the MS/MS spectra. The in-house software utilized MS/MS data in “.mgf” format as input file and parameters from a user-defined parameter.txt file to automatically perform spectral preprocessing and glycan-spectrum matching. The O-glycan MS/MS data acquired for the pooled sample in this study was searched with mass tolerances of 10 ppm for MS1 to match the accurate masses of the precursor ions and 100 ppm for MS2 to assign the diagnostic fragment ions containing single or combinations of monosaccharide residues (Hexose, HexNAc, fucose, NeuAc) and the reducing end. As shown in Supplemental Table 2, the output results from the software included high-quality MS/MS spectra for a total of 44 O-glycans from the pooled sample with the diagnostic fragment ions clearly annotated to elucidate the monosaccharide compositions and the connectivities between the monosaccharide residues.

To validate the repeatability of this protocol for the quantification of the identified O-glycans, cell surface O-glycans were released and purified from differentiated Caco-2 cells with four biological replicates. Supplemental Table 3 shows the absolute abundances and relative abundances of the O-glycans detected in Caco-2 cells and their respective averages and coefficients of variation (CVs %). The CVs of most O-glycans were less than 20% between the four replicates, demonstrating the robustness of this method for characterizing actual biological changes in O-glycans. For some O-glycans, especially the sialylated species such as H2N2S1a, H2N2S2b, and H1N1S2, the CVs were above 20% possibly because of the labile nature of the sialic acid residues, which could have dissociated during sample preparation or during in-source fragmentation. Repeatability for these compounds could be further improved by specific sialic acid derivatization techniques.<sup>48–49</sup>

### Structural Elucidation with Exoglycosidase Digestion

Tandem MS spectra provided structural information but were not sufficient to fully elucidate the structures. In the positive ion mode with CID, tandem MS data mostly provides B, Y or C, Z ions from cleavage of glycosidic bonds,<sup>2, 50</sup> and it contained

little or no cross-ring cleavages to allow linkage analysis. Digestion with exoglycosidases, guided by tandem MS data, was used to fully elucidate the structures. Exoglycosidases remove monosaccharides from the nonreducing end of the glycans depending on their specificity to the terminal monosaccharide, linkage, and anomomeric character. To reduce the sample complexity for exoglycosidase reactions, we fractionated the pooled O-glycans using off-line HPLC. Collected fractions were then analyzed on the nanoLC-chip-QTOF-MS to acquire corresponding compositions. Exoglycosidases were selected based on the compositions of each glycan. Several sequential reactions were performed to fully capture the linkages between each monosaccharides. To evaluate the completeness of the enzymatic digestion, both the accurate mass of the glycan before reaction and the appearance of the digest product are monitored using nano-chip/QTOF. There are known issues with this approach. For example, Steric hindrance may affect the digestion of galactose in the presence of an adjacent fucose.<sup>51–52</sup> Therefore, it is necessary to digest with proper fucosidase before digestion with galactosidase. Nonetheless, with this workflow we can elucidate the complete structure by combining the structural information from tandem MS data and the linkage information from the exoglycosidase digestion. We have previously used this technique for other oligosaccharides and issues regarding specificity, purity, and reactivity of the enzymes have been addressed.<sup>42, 53</sup>

In this approach, we first elucidated the small, mainly core structures obtained in the pooled sample. Supplemental Figure 4a shows the exoglycosidase digestion of Hex<sub>2</sub>HexNAc<sub>2</sub>Fuc<sub>0</sub>NeuAc<sub>0</sub> (H2N2) by β(1–4) galactosidase at the retention time 8.5 min. After digestion with β(1–4) galactosidase for 12 hours, the m/z 751.30 corresponding to Hex<sub>2</sub>HexNAc<sub>2</sub>Fuc<sub>0</sub>NeuAc<sub>0</sub> composition disappeared and a new compound with m/z 589.25 representing composition Hex<sub>1</sub>HexNAc<sub>2</sub>Fuc<sub>0</sub>NeuAc<sub>0</sub> was generated. The results indicated that the terminal galactose is β(1–4) linked. Therefore, combining tandem MS data (Supplemental Figure 4b) with linkage information, we confirmed that H2N2 represented a Core 2 structure at retention time 8.5 min. Similarly, we identified cell membrane O-glycans representing Core 1 and other core structures (Table 1). This result is in agreement with previously reported data that the majority of the human O-glycans have Core 1 and Core 2 structures.<sup>3</sup>

To elucidate the other structures, we examined the next larger structures that could yield an already elucidated smaller structures after digestion. Figure 2a shows the extracted ion chromatogram of m/z 1042.39 with the three H2N2S1 isomers detected in the O-glycan pool before structure annotation. The sequential exoglycosidase digestion of Hex<sub>2</sub>HexNAc<sub>2</sub>Fuc<sub>0</sub>NeuAc<sub>1a</sub> (H2N2S1a) at retention time 19 min with a α(2–3)sialidase and β(1–4)galactosidase are shown in Figure 2b. After digestion with α(2–3) sialidase for 1.5 hours, the m/z 1042.39 corresponding to Hex<sub>2</sub>HexNAc<sub>2</sub>Fuc<sub>0</sub>NeuAc<sub>1</sub> was consumed, and m/z 751.30 representing Hex<sub>2</sub>HexNAc<sub>2</sub>Fuc<sub>0</sub>NeuAc<sub>0</sub> appeared at 8.5 min indicating the linkage of sialic acid is α(2–3) and the remaining with composition Hex<sub>2</sub>HexNAc<sub>2</sub>Fuc<sub>0</sub>NeuAc<sub>0</sub> had a Core 2 structure. To determine the antenna where the sialic acid was attached, digestion was performed with β(1–4) galactosidase. After digestion for 12 hours, the peak corresponding to Hex<sub>2</sub>HexNAc<sub>2</sub>Fuc<sub>0</sub>NeuAc<sub>1</sub> (m/z 1042.34) disappeared and Hex<sub>1</sub>HexNAc<sub>2</sub>Fuc<sub>0</sub>NeuAc<sub>1</sub> (m/z 880.33) peak appeared at the retention time 16 min. This result showed that sialic acid was linked to the galactose in the shorter

antenna of the Core 2 structure. After combining tandem MS data with enzymatic digestion results, we confirmed the O-glycan H2N2S1a observed at 19 min was Core 2 with  $\alpha(2-3)$ -linked sialic acid that was attached to the  $\beta(1-3)$  linked galactose.

### Cell Surface O-Glycan Structure Library

This approach yielded the structures of 25 glycans representing over 85% of the total abundance (Table 1). The less abundant structures were too low in abundances to elucidate. We also identified two types of O-glycans from cell surface including O-GalNAc and O-Mannose. O-Mannosylation in human proteins has been identified before, and those glycans were elongated with GlcNAc, galactose, and sialic acid.<sup>54</sup> In this study, we identified O-mannose glycans with up to eight mannose residues that contained  $\alpha(1-2/3)$ -linked mannose polymers. The exoglycosidase digestion of H4 and H7 in Supplemental Figure 5 and Supplemental Figure 6, respectively, showed the dissociation of these hexose oligomers by  $\alpha(1-2/3)$ mannosidase presumably to mono- or disaccharides (not retained by PGC) as no oligomers with three or more hexose residues were detected in the digestion products. To our knowledge, no study has reported O-mannosylated polymers in human proteins. A potential source of O-mannosylated polymers could be a contamination from high mannose N-glycans. However, in this study, N-glycans were rigorously removed prior to releasing O-glycans. Additionally, it is not biologically possible to have polymers with seven to eight of  $\alpha(1-2/3)$ -linked mannose residues even with the largest high mannose glycan, Man9, because three of the mannose residues in Man9 are  $\alpha(1-6)$ -linked. Further studies are needed to identify the source of O-mannosylated polymers.

### Cells Surface O-Glycans Showed Large Diversity Between Cell Lines

To obtain the O-glycan profiles of different cell lines, this method was applied to three human cell lines including intestinal Caco-2 and HT-29 cells, and hepatic KKKU-213 cells. Figure 3 shows the extracted compound chromatograms (ECCs) of O-glycans from each cell line. O-Glycans were categorized into four groups including undecorated (N), sialylated (S), fucosylated (F), and fucosialylated (FS) based on the presence or the absence of sialic acid and fucose residues. Remarkably, significant differences were observed in the profiles indicating the diversity of O-glycans present in each cell line. In Caco-2, Core 2 O-glycans with one or two  $\alpha(1-6)$ -linked fucoses (H2N2F1b and H2N2F2b) were the most abundant structures. These two along with other fucosylated O-glycans represented 53.7% of the total abundance. Mono- and disialylated Core 2 O-glycans with or without terminal fucose were also identified in Caco-2 at relatively lower levels. Sialylated structures in total represented 40% of the O-glycan abundance, and approximately half of these were fucosylated. For HT-29, nearly 100% the O-glycans were sialylated, with 12% also fucosylated. The most abundant structure is the  $\alpha(2-3)$ -disialylated Core 2 O-glycan (H2N2S2b) eluting at 28 min with a relative abundance of >50%. Two similar  $\alpha(2-3)$ -sialylated Core 2 O-glycans with only one sialic acid were the second and third most abundant structures. Unlike the profiles of Caco-2 and HT-29 that were dominated by one or two most abundant structures, O-glycans identified from KKKU-M213 cells consisted of various sialylated structures and several undecorated structures. Both types included larger Core 2 glycans extended by  $\beta(1-6)$ -linked galactoses that were not detected or detected at much lower levels in the other two cell lines. In sum, KKKU-M213 cells had significantly higher (15%) undecorated O-glycans

compared to Caco-2 and HT-29, although the most abundant group was the sialylated glycans that added up to over 80% of the total abundance.

### Changes in Cell Surface Glycome during Caco-2 Cell Differentiation

Profiles of cell surface N-glycans and glycolipids from Caco-2 cells at their different growth time points during the enterocyte-like differentiation have been previously reported by our group.<sup>31, 45</sup> In this study, the same N-glycomic analysis was performed to demonstrate the reproducibility of our glycomic workflow and to compare the N-glycome of the same cells with their O-glycome. Caco-2 cells were grown in standard culture conditions and harvested at five different time points with four biological replicates for each time point: day 5, undifferentiated; day 7, confluent; day 14, partially differentiated; day 21, fully differentiated; day 24, post-differentiated. Supplemental Figure 7 shows the extracted compound chromatograms (ECCs) of the N-glycans identified from undifferentiated (day 5) and fully differentiated (day 21) Caco-2 cells, where each peak represents an N-glycan compound and the putative structures of abundant glycans are annotated. Changes in glycan types and specific glycan structures observed here were consistent with the previously reported results where the relative abundances of sialylated and fucosylated glycans significantly increased while all of the non-sialylated glycans including high mannose, and undecorated and fucosylated complex/hybrid types decreased during enterocytic differentiation.<sup>31</sup>

The remaining membrane fractions from the same Caco-2 cell samples were subjected to O-glycan analysis. As shown in Supplemental Figure 8, changes in the overall profiles of O-glycans from undifferentiated (day 5) and fully differentiated (day 21) Caco-2 cells were not as significant as those for N-glycans. Summed relative abundances of undecorated, fucosylated, sialylated, and fucosylated and sialylated O-glycans are shown in Supplemental Figure 8b with error bars illustrating standard deviations between four biological replicates. Similar to N-glycans, higher variations of O-glycan types were observed for partially differentiated cells at day 14, while when the differentiation was completed at day 21 and day 24, the relative standard deviations were minimal. Overall, a small increase in undecorated O-glycans and increase in sialylated O-glycans were observed while fucosylated O-glycans remained mostly constant during differentiation. Nonetheless, a total of 21 specific O-glycans with relative abundances higher than 0.5% were found to be significantly differentially expressed in the undifferentiated (day 5) and fully differentiated (day 21) Caco-2 cells. (Supplemental Figure 8a)

N-Glycome and O-glycome of the cell are regulated by different biosynthetic pathways and therefore may have different characteristics of changes during biological processes. With the comprehensive profiling of N-glycans and O-glycans from the same cell samples, we were able to compare for the first time the changes in the N-glycome and O-glycome during intestinal epithelial cell differentiation. Figure 4a–b shows the unique trends of changes in total sialylation and fucosylation of cell surface N- and O-glycans. While for N-glycans the total relative abundances of sialylated compounds increased significantly from  $31.2 \pm 0.7\%$  on undifferentiated Caco-2 cells (day 5) to  $64.7 \pm 3.3\%$  on fully-differentiated cell (day 21), the same group decreased from  $38.7 \pm 0.3\%$  to  $34.4 \pm 1.5\%$  for O-glycans. The total

fucosylation increased slightly from  $59.6 \pm 0.7\%$  to  $70.3 \pm 3.8\%$  for N-glycans while stayed unchanged for O-glycans.

We next compared the total intensities of cell surface N- and O-glycans per dish of cells using the total ion counts per injection, the injection volumes, and total sample volumes in Supplemental Table 4 for each sample. The total sample volumes of N- and O-glycans were optimized to obtain overall abundant and comparable ion signals of the two glycan types without saturating the detector. The estimated total intensities of Caco-2 cell surface N- and O-glycans represented by ion counts per sample are summarized in Figure 4c with error bars indicating the standard deviations between four biological replicates. Interestingly, although the N-glycan ion abundance was slightly higher than O-glycans for undifferentiated cells at day 5, the ion counts at other time points of differentiation were comparable for N-glycans and O-glycans even though N-glycans have been more extensively characterized in previous studies. The amount of both N- and O-glycans significantly (Student's t-test,  $P < 0.01$ ) increased during enterocytic differentiation (from day 5 to day 21) and remained constant after differentiation (from day 21 to day 24). This finding is consistent with the fact that brush border formation during intestinal epithelial cell differentiation significantly increases the surface area of each cell.<sup>55</sup> we can estimate that the total abundances of O-glycans and N-glycans are similar, providing potentially the first estimate of relative amounts of O- versus N-glycans. Cell surface O-glycans have long been understudied partially because it was assumed that membrane O-glycans are significantly less abundant than N-glycans.<sup>44</sup> Based on the results in this study, however, we demonstrated that cell surface O-glycans are possibly as abundant as their ion abundances are comparable to N-glycans from the same cell lines. However, because the ionization efficiencies of N- and O-glycans were potentially different, and the glycans quantified in this study may not have represented all of the glycoforms present on the cell surface, more accurate relative levels of expression of N- and O-glycans was not achievable.

## Conclusions

We constructed a comprehensive cell surface O-glycan library composed of 44 O-glycan isomers identified by MS/MS, and among them the complete structures of 25 O-glycans were elucidated by combining results from LC-MS/MS and exoglycosidase digestion. This library has been successfully used as a reference to identify and quantify O-glycans from different cell lines. The glycomic profiles of cell lines showed the highly conserved O-glycan structures and abundances between biological replicates of the same cell type and significant differences between cell types not only in monosaccharide composition level, but also in their specific core structures and linkages of extending monosaccharide residues. Unlike N-glycans that have dramatic changes in glycan groups such as high mannose and sialylated species during intestinal epithelial cell differentiation, O-glycans only have very small changes in the relative abundances of glycan types and specific structures. Such comprehensive characterization and quantitation of cell surface O-glycans would provide valuable information for studying the functions of the various glycan structures in tumor progression and the glycan-mediated cell interactions with cells, bacteria, and viruses.

## Supplementary Material

Refer to Web version on PubMed Central for supplementary material.

## Acknowledgements

Funding provided by the National Institutes of Health (R01GM049077) is gratefully acknowledged.

## References

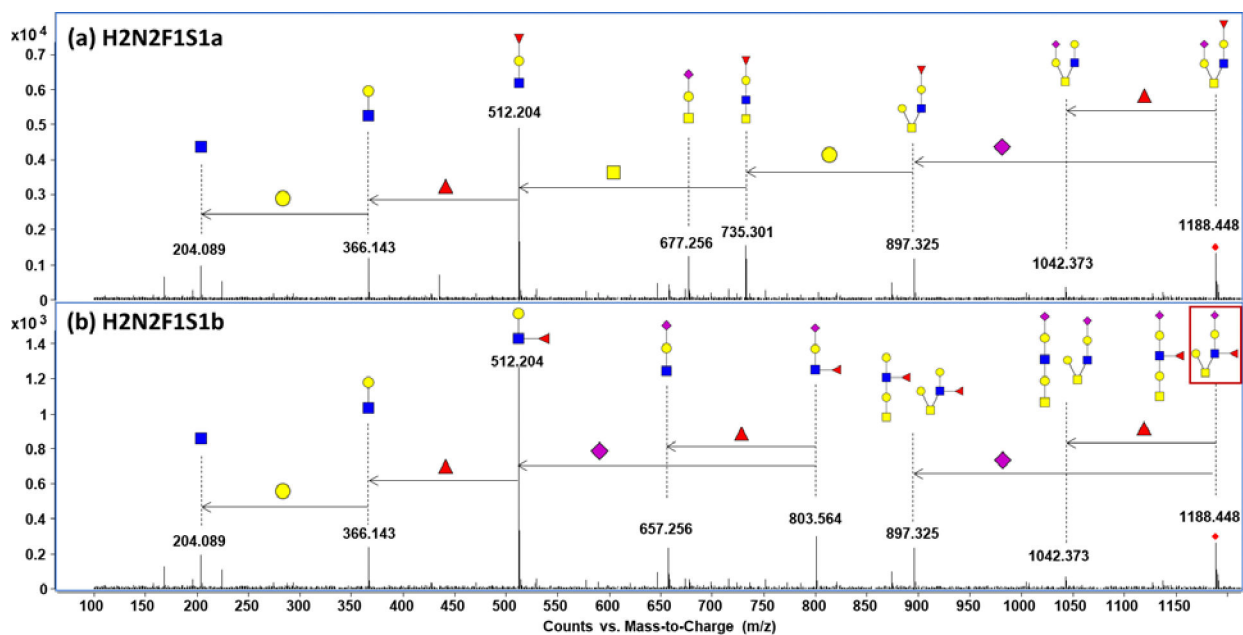
1. Spiro RG, Protein glycosylation: nature, distribution, enzymatic formation, and disease implications of glycopeptide bonds. *Glycobiology* 2002, 12 (4), 43R–56R.
2. Ruhaak LR; Xu G; Li Q; Goonatileke E; Lebrilla CB, Mass Spectrometry Approaches to Glycomic and Glycoproteomic Analyses. *Chem Rev* 2018, 118 (17), 7886–7930. [PubMed: 29553244]
3. Levery SB; Steentoft C; Halim A; Narimatsu Y; Clausen H; Vakhrushev SY, Advances in mass spectrometry driven O-glycoproteomics. *Biochim Biophys Acta* 2015, 1850 (1), 33–42. [PubMed: 25284204]
4. You X; Qin H; Ye M, Recent advances in methods for the analysis of protein o-glycosylation at proteome level. *J Sep Sci* 2018, 41 (1), 248–261. [PubMed: 28988430]
5. Fukuda M, Roles of mucin-type O-glycans in cell adhesion. *Biochim Biophys Acta* 2002, 1573 (3), 394–405. [PubMed: 12417424]
6. Lebrilla CB; An HJ, The prospects of glycan biomarkers for the diagnosis of diseases. *Mol Biosyst* 2009, 5 (1), 17–20. [PubMed: 19081926]
7. An HJ; Kronewitter SR; de Leoz ML; Lebrilla CB, Glycomics and disease markers. *Curr Opin Chem Biol* 2009, 13 (5–6), 601–7. [PubMed: 19775929]
8. Taniguchi N, Toward cancer biomarker discovery using the glycomics approach. *Proteomics* 2008, 8 (16), 3205–8. [PubMed: 18690642]
9. Kailemia MJ; Xu G; Wong M; Li Q; Goonatileke E; Leon F; Lebrilla CB, Recent Advances in the Mass Spectrometry Methods for Glycomics and Cancer. *Anal Chem* 2018, 90 (1), 208–224. [PubMed: 29049885]
10. Tsuiji H; Takasaki S; Sakamoto M; Irimura T; Hirohashi S, Aberrant O-glycosylation inhibits stable expression of dysadherin, a carcinoma-associated antigen, and facilitates cell-cell adhesion. *Glycobiology* 2003, 13 (7), 521–7. [PubMed: 12672699]
11. D'Alessandris C; Andreozzi F; Federici M; Cardellini M; Brunetti A; Ranalli M; Del Guerra S; Lauro D; Del Prato S; Marchetti P; Lauro R; Sesti G, Increased O-glycosylation of insulin signaling proteins results in their impaired activation and enhanced susceptibility to apoptosis in pancreatic beta-cells. *FASEB J* 2004, 18 (9), 959–61. [PubMed: 15059979]
12. Hatakeyama S; Kyan A; Yamamoto H; Okamoto A; Sugiyama N; Suzuki Y; Yoneyama T; Hashimoto Y; Koie T; Yamada S; Saito H; Arai Y; Fukuda M; Ohyama C, Core 2 N-acetylglucosaminyltransferase-1 expression induces aggressive potential of testicular germ cell tumor. *Int J Cancer* 2010, 127 (5), 1052–9. [PubMed: 20017138]
13. Varki A, Biological Roles of Oligosaccharides - All of the Theories Are Correct. *Glycobiology* 1993, 3 (2), 97–130. [PubMed: 8490246]
14. He Y; Xie Q; Wang Y; Liang Y; Xu X; Li Y; Miao J; Chen Z; Li Y, Liquid chromatography mass spectrometry-based O-glycomics to evaluate glycosylation alterations in gastric cancer. *Proteomics Clin Appl* 2016, 10 (2), 206–15. [PubMed: 26255982]
15. Tsuboi S; Hatakeyama S; Ohyama C; Fukuda M, Two opposing roles of O-glycans in tumor metastasis. *Trends Mol Med* 2012, 18 (4), 224–32. [PubMed: 22425488]
16. Mungul A; Cooper L; Brockhausen I; Ryder K; Mandel U; Clausen H; Rugghetti A; Miles DW; Taylor-Papadimitriou J; Burchell JM, Sialylated core 1 based O-linked glycans enhance the growth rate of mammary carcinoma cells in MUC1 transgenic mice. *Int J Oncol* 2004, 25 (4), 937–43. [PubMed: 15375543]

17. Picco G; Julien S; Brockhausen I; Beatson R; Antonopoulos A; Haslam S; Mandel U; Dell A; Pinder S; Taylor-Papadimitriou J; Burchell J, Over-expression of ST3Gal-I promotes mammary tumorigenesis. *Glycobiology* 2010, 20 (10), 1241–50. [PubMed: 20534593]
18. Thaysen-Andersen M; Packer NH, Advances in LC-MS/MS-based glycoproteomics: Getting closer to system-wide site-specific mapping of the N- and O-glycoproteome. *Bba-Proteins Proteom* 2014, 1844 (9), 1437–1452.
19. Kailemia MJ; Xu GG; Wong M; Li QY; Goonatilleke E; Leon F; Lebrilla CB, Recent Advances in the Mass Spectrometry Methods for Glycomics and Cancer. *Analytical Chemistry* 2018, 90 (1), 208–224. [PubMed: 29049885]
20. Ahn J; Bones J; Yu YQ; Rudd PM; Gilar M, Separation of 2-aminobenzamide labeled glycans using hydrophilic interaction chromatography columns packed with 1.7 $\mu$ m sorbent. *Journal of Chromatography B* 2010, 878 (3), 403–408.
21. Saldova R; Asadi Shehni A; Haakensen VD; Steinfeld I; Hilliard M; Kifer I; Helland A; Yakhini Z; Borresen-Dale AL; Rudd PM, Association of N-glycosylation with breast carcinoma and systemic features using high-resolution quantitative UPLC. *J Proteome Res* 2014, 13 (5), 2314–27. [PubMed: 24669823]
22. Ruhaak LR; Zauner G; Huhn C; Bruggink C; Deelder AM; Wuhler M, Glycan labeling strategies and their use in identification and quantification. *Anal Bioanal Chem* 2010, 397 (8), 3457–3481. [PubMed: 20225063]
23. An HJ; Miyamoto S; Lancaster KS; Kirmiz C; Li B; Lam KS; Leiserowitz GS; Lebrilla CB, Profiling of glycans in serum for the discovery of potential biomarkers for ovarian cancer. *J Proteome Res* 2006, 5 (7), 1626–35. [PubMed: 16823970]
24. Kailemia MJ; Ruhaak LR; Lebrilla CB; Amster IJ, Oligosaccharide analysis by mass spectrometry: a review of recent developments. *Anal Chem* 2014, 86 (1), 196–212. [PubMed: 24313268]
25. Ninonuevo MR; Lebrilla CB, Mass spectrometric methods for analysis of oligosaccharides in human milk. *Nutr Rev* 2009, 67 Suppl 2, S216–26. [PubMed: 19906226]
26. Shubhakar A; Kozak RP; Reiding KR; Royle L; Spencer DI; Fernandes DL; Wuhler M, Automated High-Throughput Permethylated Glycosylation Analysis of Biologics Using MALDI-TOF-MS. *Anal Chem* 2016, 88 (17), 8562–9. [PubMed: 27479043]
27. Jiang K; Zhu H; Xiao C; Liu D; Edmunds G; Wen L; Ma C; Li J; Wang PG, Solid-phase reductive amination for glycomic analysis. *Anal Chim Acta* 2017, 962, 32–40. [PubMed: 28231878]
28. Zhou S; Huang Y; Dong X; Peng W; Veillon L; Kitagawa DAS; Aquino AJA; Mechref Y, Isomeric Separation of Permethylated Glycans by Porous Graphitic Carbon (PGC)-LC-MS/MS at High Temperatures. *Anal Chem* 2017, 89 (12), 6590–6597. [PubMed: 28475308]
29. Hua S; Saunders M; Dimapasoc LM; Jeong SH; Kim BJ; Kim S; So M; Lee KS; Kim JH; Lam KS; Lebrilla CB; An HJ, Differentiation of Cancer Cell Origin and Molecular Subtype by Plasma Membrane N-Glycan Profiling. *Journal of Proteome Research* 2014, 13 (2), 961–968. [PubMed: 24303873]
30. Park D; Arabyan N; Williams CC; Song T; Mitra A; Weimer BC; Maverakis E; Lebrilla CB, Salmonella Typhimurium Enzymatically Landscapes the Host Intestinal Epithelial Cell (IEC) Surface Glycome to Increase Invasion. *Mol Cell Proteomics* 2016, 15 (12), 3653–3664. [PubMed: 27754876]
31. Park D; Brune KA; Mitra A; Marusina AI; Maverakis E; Lebrilla CB, Characteristic Changes in Cell Surface Glycosylation Accompany Intestinal Epithelial Cell (IEC) Differentiation: High Mannose Structures Dominate the Cell Surface Glycome of Undifferentiated Enterocytes. *Mol Cell Proteomics* 2015, 14 (11), 2910–2921. [PubMed: 26355101]
32. Ruhaak LR; Stroble C; Dai JL; Barnett M; Taguchi A; Goodman GE; Miyamoto S; Gandara D; Feng ZD; Lebrilla CB; Hanash S, Serum Glycans as Risk Markers for Non-Small Cell Lung Cancer. *Cancer Prev Res* 2016, 9 (4), 317–323.
33. Chen YZ; Tang YR; Sheng ZY; Zhang Z, Prediction of mucin-type O-glycosylation sites in mammalian proteins using the composition of k-spaced amino acid pairs. *BMC Bioinformatics* 2008, 9, 101. [PubMed: 18282281]
34. Mulagapati S; Koppolu V; Raju TS, Decoding of O-Linked Glycosylation by Mass Spectrometry. *Biochemistry* 2017, 56 (9), 1218–1226. [PubMed: 28196325]

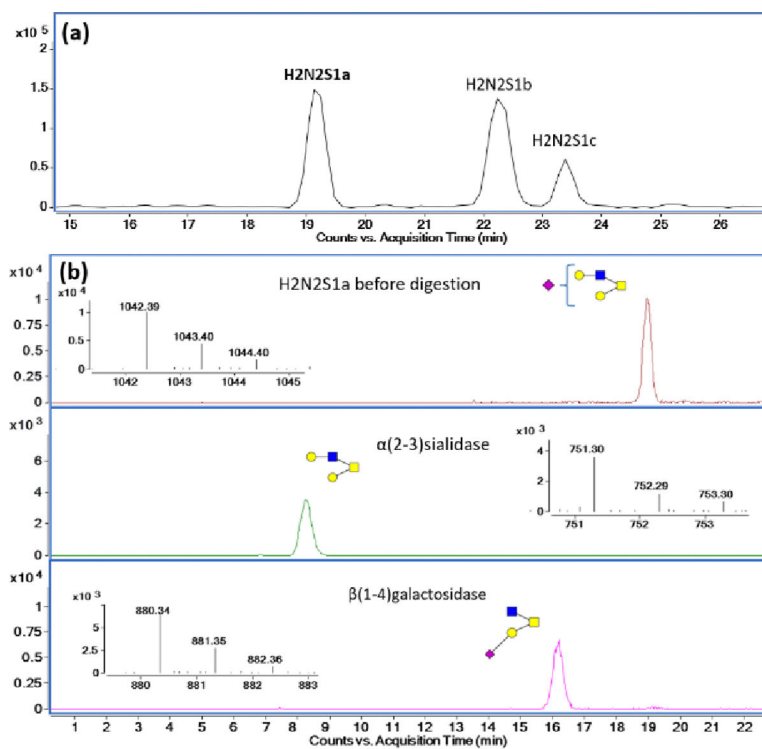
35. Park DD; Xu G; Wong M; Phoomak C; Liu M; Haigh NE; Wongkham S; Yang P; Maverakis E; Lebrilla CB, Membrane glycomics reveal heterogeneity and quantitative distribution of cell surface sialylation. *Chem Sci* 2018, 9 (29), 6271–6285. [PubMed: 30123482]
36. Morelle W; Michalski JC, Analysis of protein glycosylation by mass spectrometry. *Nat Protoc* 2007, 2 (7), 1585–602. [PubMed: 17585300]
37. Yang S; Hoti N; Yang W; Liu Y; Chen L; Li S; Zhang H, Simultaneous analyses of N-linked and O-linked glycans of ovarian cancer cells using solid-phase chemoenzymatic method. *Clin Proteomics* 2017, 14, 3. [PubMed: 28100988]
38. Yang S; Hu Y; Sokoll L; Zhang H, Simultaneous quantification of N- and O-glycans using a solid-phase method. *Nat Protoc* 2017, 12 (6), 1229–1244. [PubMed: 28518173]
39. de Leoz ML; Young LJ; An HJ; Kronewitter SR; Kim J; Miyamoto S; Borowsky AD; Chew HK; Lebrilla CB, High-mannose glycans are elevated during breast cancer progression. *Mol Cell Proteomics* 2011, 10 (1), M110 002717.
40. Allam H; Aoki K; Benigno BB; McDonald JF; Mackintosh SG; Tiemeyer M; Abbott KL, Glycomic analysis of membrane glycoproteins with bisecting glycosylation from ovarian cancer tissues reveals novel structures and functions. *J Proteome Res* 2015, 14 (1), 434–46. [PubMed: 25437919]
41. Wu S; Salcedo J; Tang N; Waddell K; Grimm R; German JB; Lebrilla CB, Employment of tandem mass spectrometry for the accurate and specific identification of oligosaccharide structures. *Anal Chem* 2012, 84 (17), 7456–62. [PubMed: 22867103]
42. Song T; Aldredge D; Lebrilla CB, A Method for In-Depth Structural Annotation of Human Serum Glycans That Yields Biological Variations. *Anal Chem* 2015, 87 (15), 7754–62. [PubMed: 26086522]
43. Song T; Ozcan S; Becker A; Lebrilla CB, In-depth method for the characterization of glycosylation in manufactured recombinant monoclonal antibody drugs. *Anal Chem* 2014, 86 (12), 5661–6. [PubMed: 24828102]
44. An HJ; Gip P; Kim J; Wu S; Park KW; McVaugh CT; Schaffer DV; Bertozzi CR; Lebrilla CB, Extensive determination of glycan heterogeneity reveals an unusual abundance of high mannose glycans in enriched plasma membranes of human embryonic stem cells. *Mol Cell Proteomics* 2012, 11 (4), M111 010660.
45. Wong M; Xu G; Park D; Barboza M; Lebrilla CB, Intact glycosphingolipidomic analysis of the cell membrane during differentiation yields extensive glycan and lipid changes. *Sci Rep* 2018, 8 (1), 10993. [PubMed: 30030471]
46. An HJ; Lebrilla CB, Structure elucidation of native N- and O-linked glycans by tandem mass spectrometry (tutorial). *Mass Spectrom Rev* 2011, 30 (4), 560–78. [PubMed: 21656841]
47. Liu Y; Clemmer DE, Characterizing oligosaccharides using injected-ion mobility/mass spectrometry. *Anal Chem* 1997, 69 (13), 2504–9. [PubMed: 21639386]
48. Yang S; Jankowska E; Kosikova M; Xie H; Cipollo J, Solid-Phase Chemical Modification for Sialic Acid Linkage Analysis: Application to Glycoproteins of Host Cells Used in Influenza Virus Propagation. *Anal Chem* 2017, 89 (17), 9508–9517. [PubMed: 28792205]
49. Wheeler SF; Domann P; Harvey DJ, Derivatization of sialic acids for stabilization in matrix-assisted laser desorption/ionization mass spectrometry and concomitant differentiation of alpha(2 --> 3)- and alpha(2 --> 6)-isomers. *Rapid Commun Mass Spectrom* 2009, 23 (2), 303–12. [PubMed: 19089860]
50. Domon B; Costello CE, A Systematic Nomenclature for Carbohydrate Fragmentations in Fab-Ms Ms Spectra of Glycoconjugates. *Glycoconjugate J* 1988, 5 (4), 397–409.
51. Tao N; DePeters EJ; Freeman S; German JB; Grimm R; Lebrilla CB, Bovine milk glycome. *J Dairy Sci* 2008, 91 (10), 3768–78. [PubMed: 18832198]
52. Wu S; Tao N; German JB; Grimm R; Lebrilla CB, Development of an annotated library of neutral human milk oligosaccharides. *J Proteome Res* 2010, 9 (8), 4138–51. [PubMed: 20578730]
53. Aldredge D; An HJ; Tang N; Waddell K; Lebrilla CB, Annotation of a serum N-glycan library for rapid identification of structures. *J Proteome Res* 2012, 11 (3), 1958–68. [PubMed: 22320385]



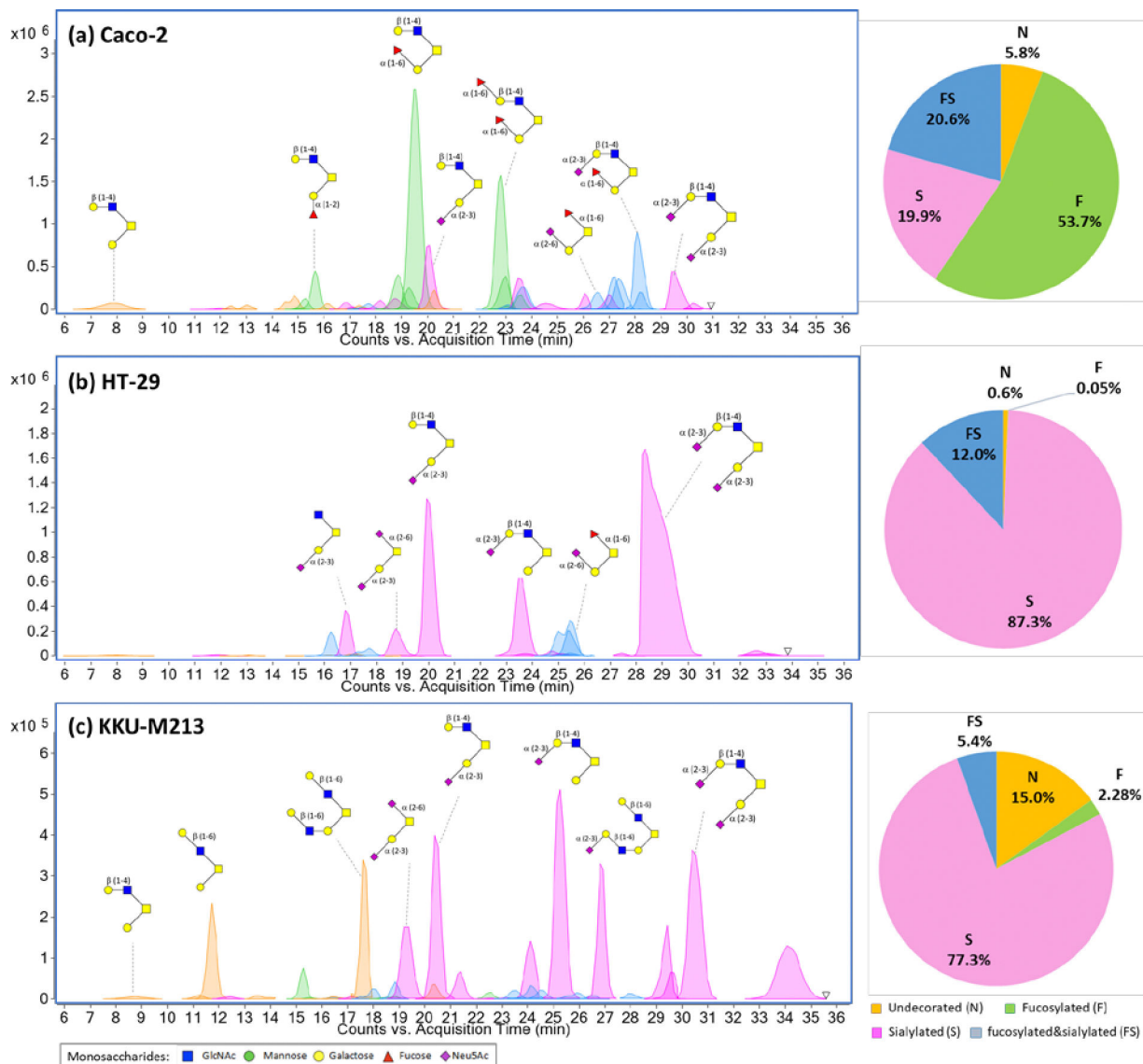
54. Vester-Christensen MB; Halim A; Joshi HJ; Steentoft C; Bennett EP; Lavery SB; Vakhrushev SY; Clausen H, Mining the O-mannose glycoproteome reveals cadherins as major O-mannosylated glycoproteins. *Proc Natl Acad Sci U S A* 2013, 110 (52), 21018–23. [PubMed: 24101494]
55. Hidalgo IJ; Raub TJ; Borchardt RT, Characterization of the human colon carcinoma cell line (Caco-2) as a model system for intestinal epithelial permeability. *Gastroenterology* 1989, 96 (3), 736–49. [PubMed: 2914637]



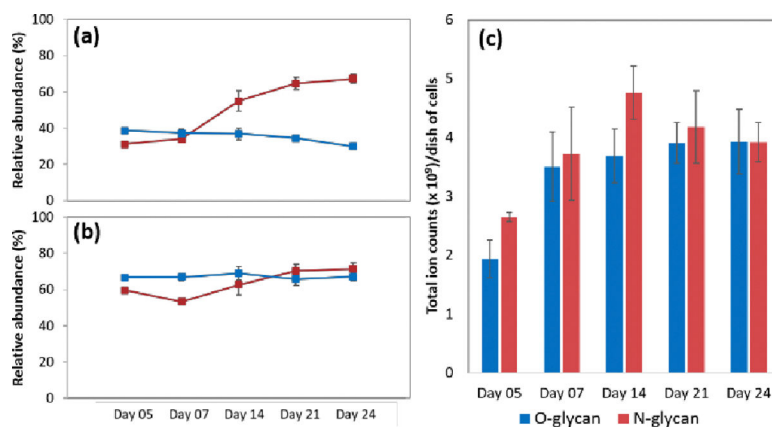
**Figure 1.** Annotated tandem mass spectra of two isomers with monosaccharide composition  $\text{Hex}_2\text{HexNAc}_2\text{Fuc}_1\text{NeuAc}_1$  (a)  $\text{Hex}_2\text{HexNAc}_2\text{Fuc}_1\text{NeuAc}_1\text{a}$  (H2N2F1S1a) at retention time 16.6 min (b)  $\text{Hex}_2\text{HexNAc}_2\text{Fuc}_1\text{NeuAc}_1\text{b}$  (H2N2F1S1b) at retention time 22.5 min, with the actual structure confirmed by exoglycosidase digestion indicated in the red box.



**Figure 2.** Extracted ion chromatograms of (a)  $m/z$  1042.39 from unfractionated O-glycan pool with the H2N2S1 isomers annotated; (b) H2N2S1a in fraction #65 before exoglycosidase digestion and its corresponding products after digestion with  $\alpha(2-3)$  sialidase and  $\beta(1-4)$  galactosidase.



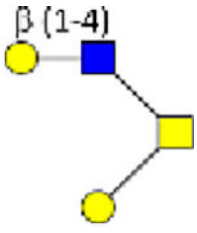
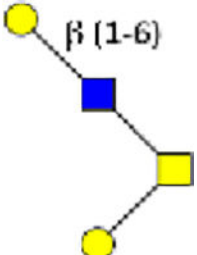
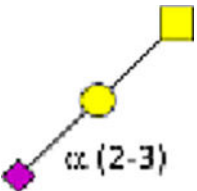
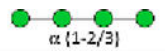
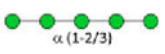
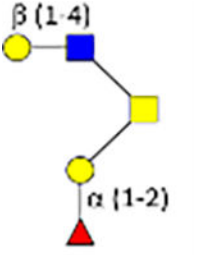

**Figure 3.** Extracted compound chromatograms of cell surface O-glycans with the abundant elucidated structures annotated and pie charts representing the relative abundances of each glycan type from (a) Caco-2, (b) HT-29, (c) KKU-M213.

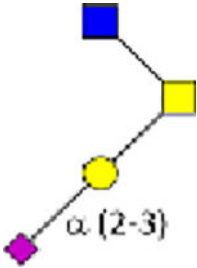
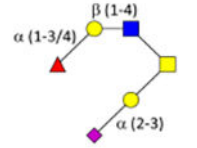
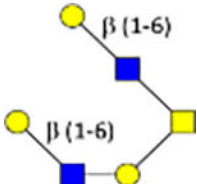
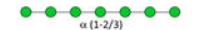
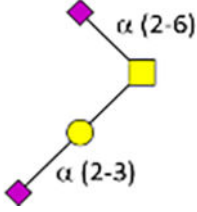
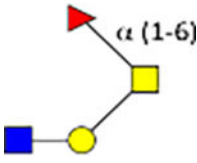
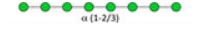


**Figure 4.** Comparison of Caco-2 cell surface N- and O-glycans during differentiation. (a) Differential changes in total sialylation (sialylated + fucosialylated). (b) Differential changes in total fucosylation (fucosylated + fucosialylated). (c) Total ion counts of cell surface N- and O-glycans.

**Table 1.**

Elucidated structures of 25 cell surface O-glycans

Composition	Name	Experimental Mass	Theoretical Mass	Error (ppm)	RT (min)	Structure	Relative Abundance
Hex <sub>2</sub> HexNAc <sub>2</sub>	H2N2a	750.291	750.291	0.666	8.5		4.6%
Hex <sub>2</sub> HexNAc <sub>2</sub>	H2N2b	750.291	750.291	0.933	11.2		3.0%
Hex <sub>1</sub> HexNAc <sub>1</sub> NeuAc <sub>1</sub>	H1N1S1	676.258	676.258	0.887	11.7		1.2%
Hex <sub>4</sub>	H4	668.240	668.240	-1.048	9.0		0.2%
Hex <sub>5</sub>	H5	830.291	830.290	1.445	13.5		3.8%
Hex <sub>2</sub> HexNAc <sub>2</sub> Fuc <sub>1</sub>	H2N2F1a	896.349	896.349	0.112	15.5		2.1%
Hex <sub>6</sub>	H6	992.344	992.343	1.411	15.0		2.6%

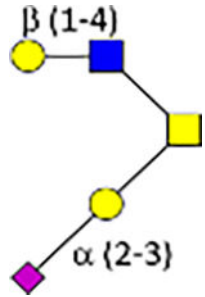
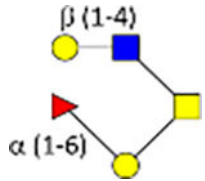
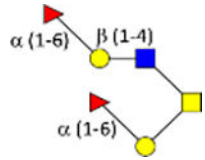
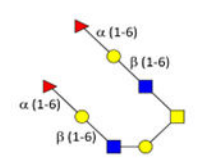
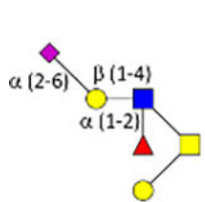
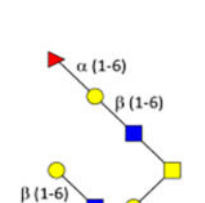
Composition	Name	Experimental Mass	Theoretical Mass	Error (ppm)	RT (min)	Structure	Relative Abundance
Hex <sub>1</sub> HexNAc <sub>2</sub> NeuAc <sub>1</sub>	H1N2S1	879.334	879.333	0.682	16.0		1.4%
Hex <sub>2</sub> HexNAc <sub>2</sub> Fuc <sub>1</sub> NeuAc <sub>1</sub>	H2N2F1S1a	1187.443	1187.444	-0.505	16.6		0.5%
Hex <sub>3</sub> HexNAc <sub>3</sub>	H3N3a	1115.429	1115.426	2.241	17.0		0.6%
Hex <sub>7</sub>	H7	1154.396	1154.396	-0.260	16.0		0.8%
Hex <sub>1</sub> HexNAc <sub>1</sub> NeuAc <sub>2</sub>	H1N1S2	967.348	967.349	-0.930	17.7		6.5%
Hex <sub>1</sub> HexNAc <sub>2</sub> Fuc <sub>1</sub>	H1N2F1	734.299	734.298	1.362	18.0		2.3%
Hex <sub>8</sub>	H8	1316.450	1316.449	0.456	17.2		0.2%

Author Manuscript

Author Manuscript

Author Manuscript

Author Manuscript

Composition	Name	Experimental Mass	Theoretical Mass	Error (ppm)	RT (min)	Structure	Relative Abundance
Hex <sub>2</sub> HexNAc <sub>2</sub> NeuAc <sub>1</sub>	H2N2S1a	1041.386	1041.386	0.096	19.1		6.4%
Hex <sub>2</sub> HexNAc <sub>2</sub> Fuc <sub>1</sub>	H2N2F1b	896.351	896.349	2.454	19.0		22.1%
Hex <sub>2</sub> HexNAc <sub>2</sub> Fuc <sub>2</sub>	H2N2F2b	1042.403	1042.406	-2.494	22.0		10.8%
Hex <sub>3</sub> HexNAc <sub>3</sub> Fuc <sub>2</sub>	H3N2F2	1407.542	1407.540	1.279	22.4		0.2%
Hex <sub>2</sub> HexNAc <sub>2</sub> Fuc <sub>1</sub> NeuAc <sub>1</sub>	H2N2F1S1b	1187.437	1187.439	-1.659	22.5		1.2%
Hex <sub>3</sub> HexNAc <sub>3</sub> Fuc <sub>1</sub>	H3N3F1	1261.479	1261.481	-1.268	22.8		0.5%

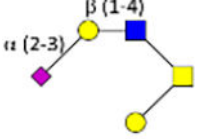
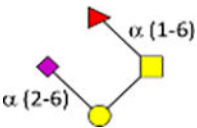
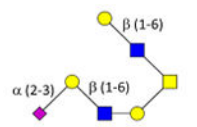
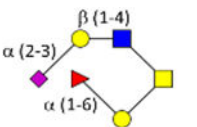
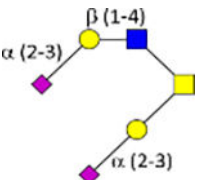
Author Manuscript

Author Manuscript

Author Manuscript

Author Manuscript



Composition	Name	Experimental Mass	Theoretical Mass	Error (ppm)	RT (min)	Structure	Relative Abundance
Hex <sub>2</sub> HexNAc <sub>2</sub> NeuAc <sub>1</sub>	H2N2S1c	1041.386	1041.386	-0.384	23.5		2.0%
Hex <sub>1</sub> HexNAc <sub>1</sub> Fuc <sub>1</sub> NeuAc <sub>1</sub>	H1N1F1S1a	822.312	822.312	0.486	24.0		2.4%
Hex <sub>3</sub> HexNAc <sub>3</sub> NeuAc <sub>1</sub>	H3N3S1	1406.518	1406.518	0.000	25.0		0.9%
Hex <sub>2</sub> HexNAc <sub>2</sub> Fuc <sub>1</sub> NeuAc <sub>1</sub>	H2N2F1S1c	1187.444	1187.444	0.084	27.0		0.7%
Hex <sub>2</sub> HexNAc <sub>2</sub> NeuAc <sub>2</sub>	H2N2S2b	1332.480	1332.481	-0.750	28.0		8.3%

Author Manuscript

Author Manuscript

Author Manuscript

Author Manuscript